ISSN 0030-400X, Optics and Spectroscopy, 2019, Vol. 126, No. 4, pp. 341–345. © Pleiades Publishing, Ltd., 2019.
Russian Text © The Author(s), 2019, published in Optika i Spektroskopiya, 2019, Vol. 126, No. 4, pp. 423–427.

SPECTROSCOPY OF CONDENSED STATES

Manifestations of Structural Phase Transitions in a Rb_2KLuF_6 Crystal in Its Raman Spectra

A. S. Krylov[a, *], A. N. Vtyurin[a, b], V. N. Voronov[a], and S. N. Krylova[a]

[a] *Kirensky Institute of Physics, Siberian Branch, Russian Academy of Sciences, Krasnoyarsk, 660036 Russia*
[b] *Siberian Federal University, Krasnoyarsk, 660041 Russia*
**e-mail: slanky@iph.krasn.ru*

Received October 15, 2018; revised October 15, 2018; accepted December 28, 2018

Abstract—The Raman spectra of an Rb_2KLuF_6 crystal are studied in the temperature range from 8 to 375 K, which includes two phase transitions: one of which proceeds from a cubic to a tetragonal phase, while the other transition takes place from a tetragonal to a monoclinic phase. An analysis of the temperature dependences of parameters of spectral lines shows that the former transition is of the second kind, while the latter transition is of the first kind, close to the tricritical point. It is shown that the structural phase transitions in the Rb_2KLuF_6 double perovskite are not associated with disordering. The former transition is associated with rotations of LuF_6 octahedra around the fourth-order axis, while the latter transition is related with rotations of octahedra and displacements of rubidium ions.

DOI: 10.1134/S0030400X1904012X

INTRODUCTION

Crystals with the general formula $Rb_2KRe^{(3+)}F_6$ belong to the extensive family of elpasolites (double perovskites) $A_2B^{(1)}B^{(2)}X_6$, where A and B are cations of metals or more complex molecular ions and X refers to anions of oxygen or halogens. Cations B in the cubic structure of elpasolites occupy ideal octahedral positions. Special interest from researchers in elpasolites is caused by the creation of new functional materials [1]. These can be crystals for creating solar cells [2–4] and semiconductors [5]. Crystals of this family are ideal matrices for creating laser media based on transitions of metals and rare-earth ions in an octahedral environment [6–9].

The cubic structure of halogen elpasolites is unstable at low temperatures, and they undergo ferroelastic phase transitions upon cooling [10–15]. A decrease in cation radius $Re^{(3+)}$ leads to a change in the sequence of transitions from $Fm3m–P12_1/n1$ for $Re^{(3+)}$ = Ho, Dy, and Tb to $Fm3m–I4/m–P12_1/nl$ for $Re^{(3+)}$ = In, Sc, and Lu [12]. Transitions in Rb_2KInF_6 and Rb_2KScF_6 are associated with small rotations of ReF_6 octahedra and displacements of rubidium ions [13–17]. These transitions are of the displacive type and are accompanied by the condensation of the soft phonon mode in the cubic phase. In isostructural elpasolites Rb_2KHoF_6 and Rb_2KDyF_6, structural phase transitions of the first kind were observed [12, 18, 19]. The total change in the entropy of a crystal upon transition from a cubic to a monoclinic phase depends on the size of the $Re^{(3+)}$ ion and decreases from $1.3R$ (Ho) to $0.7R$ (Sc) [16]. The maximum magnitude of this change (1.3R), although being quite large, does not allow one to relate these transitions to ordering processes. In this connection, it becomes interesting to investigate these transitions in crystals of this family with other rare-earth ions and to perform a comparative analysis of data on several fluorides in order to clarify mechanisms by which observed phase transitions proceed. Raman scattering spectroscopy seems to be an efficient experimental tool to establish both the nature of observed phase transitions and their mechanism, as well as the role played by individual structural units [20, 21].

EXPERIMENTAL

Rb_2KLuF_6 crystals were synthesized by the solid-state reaction method from a mixture of RbF, KF, and LuF_3 fluorides, which was carried out in a platinum ampoule in an argon atmosphere.

The Raman spectra of an Rb_2KLuF_6 crystal were examined in the temperature range of 8–390 K. The spectra were recorded in the backscattering geometry using a Jobin Yvon T64000 triple spectrometer in the dispersion subtraction mode with a CCD detector cooled to 140 K. The spectral resolution was 2 cm^{-1} (diffraction gratings with 1800 g/mm; 100-μm slits). The spectra were excited by the line at 514.5 nm of a Spectra-Physics Stabilite 2017 single-mode Ar^+ laser; the radiation power on a sample was 5 mW. Tempera-

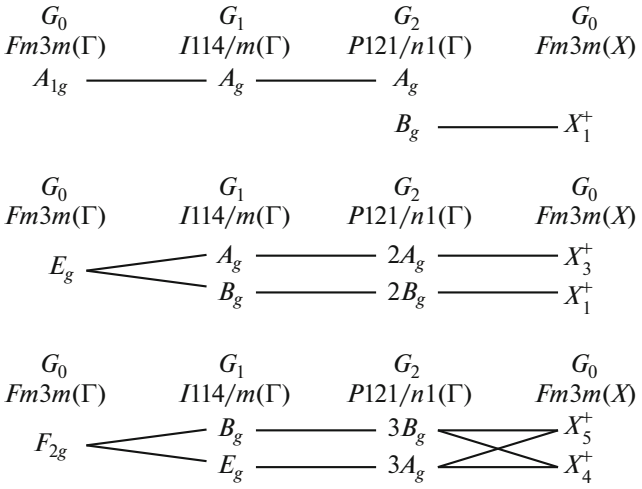

Fig. 1. Correlation diagrams for internal vibrations of ReF_6 octahedra in the cubic, tetragonal, and monoclinic phases of elpasolites.

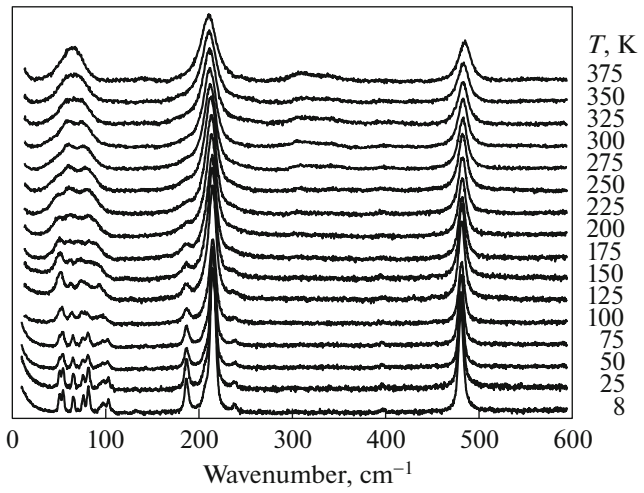

Fig. 2. Temperature transformation of the Raman spectrum of Rb_2KLuF_6.

ture measurements were performed using an ARS CS204-X1_SS cryostat with a temperature step of 0.5 K. The protocol of our temperature measurements was similar to that described in [22]. To determine the numerical values of parameters of the spectral lines, the procedure for deconvolution of spectral lines into contours was applied. The Lorentz function was used as a model contour.

RESULTS AND DISCUSSION

Upon cooling, an Rb_2KLuF_6 crystal undergoes two phase transitions: one from a cubic to a tetragonal phase ($I114/m$, $Z = 2$), which occurs at 370 K, and the other to a monoclinic phase ($P12_1/n1$, $Z = 2$), which proceeds at 366 K [23, 24].

The vibrational representation at the center of the Brillouin zone of the cubic phase has the form

$$\Gamma_{\text{vibr}}(Fm{-}3m) = A_{1g}(xx, yy, zz) + E_g(xx, yy, zz) + 2F_{2g}(xz, yz, xy) + F_{1g} + 5E_{1u} + F_{2u}. \quad (1)$$

In the tetragonal phase,

$$\Gamma_{\text{vibr}}(I114/m) = 3A_g(xx, yy, zz) + 3B_g(xx, yy, xy) + 3E_g(xz, yz) + 5A_u + 6E_u + B_u. \quad (2)$$

In the monoclinic phase,

$$\Gamma_{\text{vibr}}(P12_1/n1) = 12A_g(xx, yy, zz, xy, yx) + 12B_g(xz, yz, zx, zy) + 18A_u + 18B_u. \quad (3)$$

Here, the corresponding components of the Raman scattering tensor are given in the parentheses.

The correlation diagrams for the Raman active modes are shown in Fig. 1. The transition from the cubic phase to the tetragonal one occurs without a change in the volume of the primitive cell, and the expected increase in the number of spectral lines occurs only due to the lowering of symmetry and because of a partial removal of the degeneracy of triply degenerate vibrations. The transition to the monoclinic phase is accompanied by a doubling of the volume of the primitive cell, as a result of which, apart from the complete removal of the degeneracy, modes from point $X(0, 0, \pi/a)$ of the Brillouin zone of the cubic phase are additionally activated in the spectrum.

The temperature transformation of the entire Raman spectrum is shown in Fig. 2. The spectrum of the cubic phase (375 K) can be divided into four ranges, which correspond to vibrations of structural units: the range of lattice vibrations lies below 100 cm^{-1}; the range 150–250 cm^{-1} corresponds to bending vibrations of F–Lu–F bonds; the range of 250–400 cm^{-1} refers to Lu–F stretching vibrations, and the range of 470–490 cm^{-1} corresponds to Lu–F totally symmetric stretching vibrations. Note that the intensity of the Lu–F stretching vibration of the E_g type is extremely low, and the quantitative analysis of its parameters is difficult. Table 1 shows the assignment and experimental frequencies of corresponding modes of the cubic phase for the Rb_2KLuF_6, Rb_2KScF_6, Rb_2KInF_6, Rb_2KHoF_6, and Rb_2KDyF_6 crystals. In the cubic phase of the examined Rb_2KLuF_6 crystal, which is stable above 370 K, three lines were reliably observed: 484, 210, and 62 cm^{-1} (Fig. 2). The lines at 484 and 210 cm^{-1} correspond to internal vibrations of LuF_6 octahedra; the line at 62 cm^{-1} (at 375 K) corresponds to a single active lattice vibration. The positions of these lines in Rb_2KLuF_6 only insignificantly differ from those in the spectra of the isomorphic Rb_2KScF_6, Rb_2KInF_6, Rb_2KHoF_6, and Rb_2KDyF_6 crystals. Lowering the temperature leads to a noticeable decrease in the width of the lines, and below the

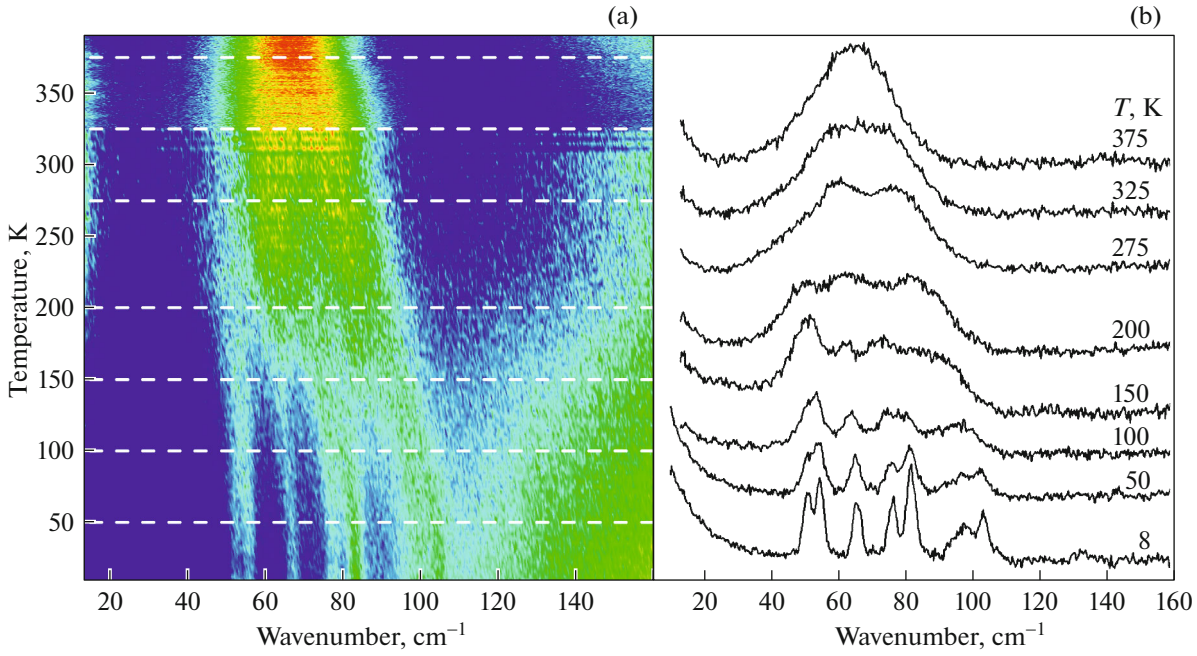

Fig. 3. (a) Raman scattering intensity distribution of an Rb_2KLuF_6 crystal in the low-frequency range; (b) temperature transformation of the low-frequency range of the spectrum. Dashed lines indicate the temperatures at which the spectra in Fig. 3b were measured.

temperatures of the phase transitions, to the appearance of new lines in accordance with the selection rules.

Figure 3a presents the intensity pattern of the low-frequency range of the spectrum in relation to the temperature. The dashed lines show the temperatures that correspond to the spectra shown in Fig. 3b. The intensity of the F_{2g} lattice mode decreases with decreasing temperature, and this mode becomes split in accordance with the selection rules. The spectral transformation in the same range is shown in Fig. 3b. Both the appearance of new lines due to an increase in the volume of the primitive cell after the transition from the tetragonal to the monoclinic phase and the splitting of lines due to the removal of the degeneracy after the phase transitions can be clearly seen. At the same time, a large number of interacting low-frequency lattice modes associated both with vibrations of rubidium ions and with librations of LuF_6 octahedra leads to the fact no restoration of soft modes below the phase transitions is observed, in contrast to crystals with ScF_6, InF_6, and YF_6 octahedral groups [13, 14].

Figure 4 shows the temperature dependences of the position and halfwidth (FWHM) of the line that corresponds to the totally symmetric stretching vibration of the LuF_6 octahedron. Previous studies [13, 14, 25] have shown that, in Rb_2KScF_6, Rb_2KInF_6, and Rb_2NaYF_6 crystals, the dependences of the position of the line corresponding to the totally symmetric internal vibration of the octahedral group changes monotonically with temperature upon phase transition. However, the phase transition at 367 K in the Rb_2KLuF_6 crystal under study is accompanied by a small jump in the frequency of the line at 483 cm^{-1} upon the transition from the tetragonal to the monoclinic phase (Fig. 4a), although the linewidth also changes monotonically (Fig. 4b). This behavior corre-

Table 1. Symmetry species and positions of lines in Raman spectra of cubic phases of $Rb_2KB^{(3+)}F_6$ crystals

Symmetry species	Rb_2KLuF_6, cm^{-1}	[10] Rb_2KHoF_6, cm^{-1}	[10] Rb_2KDyF_6, cm^{-1}	[11] Rb_2KScF_6, cm^{-1}	[12] Rb_2KInF_6, cm^{-1}	[13] Rb_2KYF_6, cm^{-1}
A_{1g}	484	472	470	505	507	470
E_g			380	390	379	
F_{2g}	210	204	202	230	218	210
F_{2g}	62	61	65	89	69	60

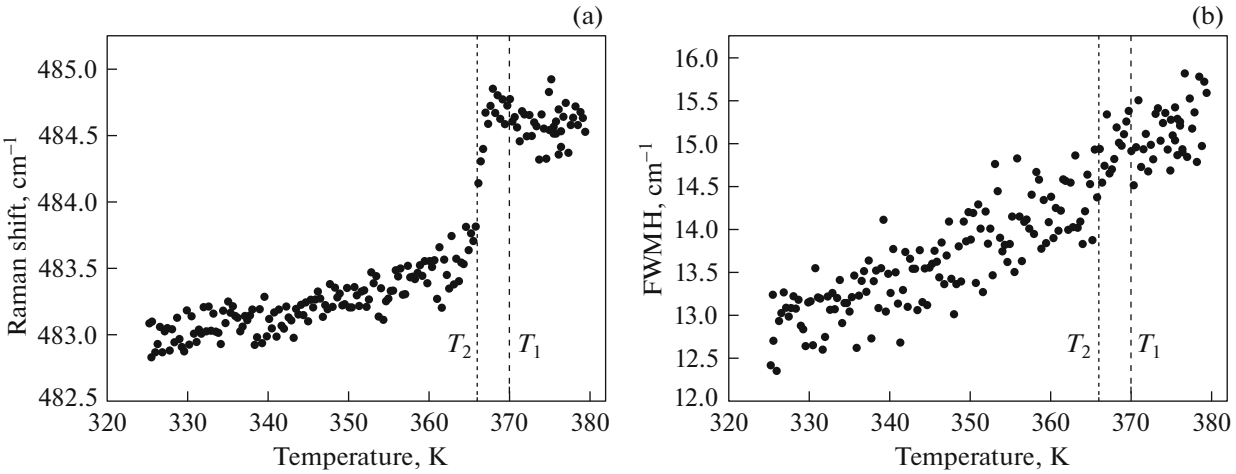

Fig. 4. Temperature behavior of the parameters of the totally symmetric vibration: (a) position and (b) linewidth (FWHM).

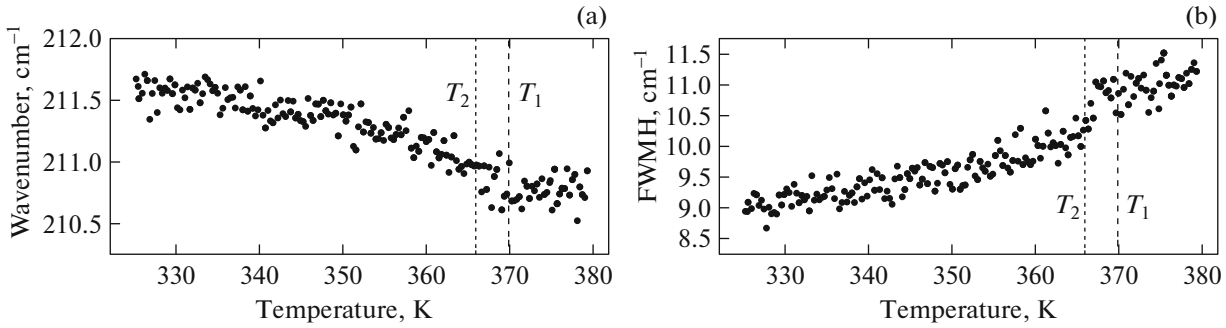

Fig. 5. Temperature behavior of the parameters of the internal F_{2g} vibration: (a) position and (b) linewidth (FWHM).

sponds to a first-order phase transition that is close to the tricritical point.

The temperature dependences of the position and the width of the line corresponding to the F_{2g} internal bending vibration of the LuF_6 octahedron are shown in Fig. 5. Upon cooling below 370 K, the position of this line changes from 211.5 to 210.5 cm^{-1}, and another two lines appear near this line—at 186 and 237 cm^{-1} (Fig. 1). The width of the line at 211 cm^{-1} monotonically decreases with cooling. The temperature dependence of the width experiences a kink upon transition from the tetragonal to the monoclinic phase (Fig. 5b). In accordance with the selection rules, one can expect that, in the monoclinic phase, this line will split due to the degeneracy removal, and additional lines will emerge that arrived from the boundary of the Brillouin zone of the cubic phase. It is clear that the observed additional lines are caused precisely by such an activation, whereas the magnitude of the splitting does not allow one to observe additional lines near the transition from the cubic to the tetragonal phase. Therefore, the splitting is fixed significantly lower in temperature after the phase transition.

CONCLUSIONS

Therefore, we can conclude that the transition from the cubic to the tetragonal phase is a transition of the second kind, whereas the transition from the tetragonal to the monoclinic phase is of the first kind, and it is close to the tricritical point. Similarly to other isomorphic fluorides with an elpasolite structure [12], the former transition is associated with the rotation of LuF_6 octahedra around the fourth-order axis, whereas the latter transition is associated with the rotation of octahedra and displacements of rubidium ions. Below this transition, strong interactions of restoring soft modes with other low-frequency lattice vibrations and fluctuations of second-order parameters become possible [26, 27]; as a result of which these modes are not observed separately. Small halfwidths of lines and their temperature dependences correspond to the decay of phonons due to anharmonicity and are not associated with structural disordering.

FUNDING

This work was supported by the Russian Foundation for Basic Research, project nos. 16-02-00102, 18-02-00754.

REFERENCES

1. Xin-Gang Zhao, Dongwen Yang, Ji-Chang Ren, Yuanhui Sun, Zewen Xiao, and Lijun Zhang, Joule **2**, 1662 (2018). https://doi.org/10.1016/j.joule.2018.06.017
2. J. A. Steele, P. Puech, M. Keshavarz, R. X. Yang, S. Banerjee, E. Debroye, C. W. Kim, H. F. Yuan, N. H. Heo, J. Vanacken, A. Walsh, J. Hofkens, and M. B. J. Roeffaers, ACS Nano **12**, 8081 (2018).
3. N. Singhal, R. Chakraborty, P. Ghosh, and A. Nag, Chem. Asian J. **13**, 2085 (2018).
4. M. Pantaler, K. T. Cho, V. I. E. Queloz, I. G. Benito, C. Fettkenhauer, I. Anusca, M. K. Nazeeruddin, D. C. Lupascu, and G. Grancini, ACS Energy Lett. **3**, 1781 (2018).
5. S. E. Creutz, E. N. Crites, M. C. de Siena, and D. R. Gamelin, Nano Lett. **18**, 1118 (2018).
6. A. S. Aleksandrovsky, A. S. Krylov, A. V. Malakhovskii, and V. N. Voronov, J. Lumin. **132**, 690 (2012).
7. M. A. Buñuel, B. Moine, and B. Jacquier, J. Appl. Phys. **86**, 5045 (1999).
8. L. Cornu Lucile, M. Gaudon, O. Toulemonde, P. Veber, and V. Jubera, Dalton Trans. **45**, 3380 (2016).
9. A. M. Woods, R. S. Sinkovits, J. C. Charpie, W. L. Huang, R. H. Bartram, and A. R. Rossi, J. Phys. Chem. Solids **54**, 543 (1993).
10. I. N. Flerov, M. V. Gorev, K. S. Aleksandrov, A. Tressaud, J. Grannec, and M. Couzi, Mater. Sci. Eng. R **24**, 81 (1998).
11. A. Vtyurin, A. Krylov, V. Voronov, and S. Krylova, Ferroelectrics **512**, 58 (2017).
12. S. N. Krylova, A. N. Vtyurin, A. Bulou, A. S. Krylov, and N. G. Zamkova, Phys. Solid State **46**, 1311 (2004).
13. A. S. Krylov, S. N. Krylova, A. N. Vtyurin, V. N. Voronov, and A. S. Oreshonkov, Ferroelectrics **416**, 95 (2011).
14. M. Couzi, S. Khaïroun, and A. Tressaud, Phys. Status Solidi A **98**, 423 (1986).
15. E. G. Maksimov, V. I. Zinenko, and N. G. Zamkova, Phys. Usp. **47**, 1075 (2004).
16. I. N. Flerov, M. V. Gorev, K. S. Aleksandrov, A. Tressaud, and V. D. Fokina, Crystallogr. Rep. **49**, 100 (2004).
17. A. S. Krylov, A. Bulou, S. N. Krylova, V. N. Voronov, A. N. Vtyurin, and N. G. Zamkova, Comput. Mater. Sci. **36**, 221 (2006).
18. B. V. Beznosikov, I. N. Flerov, M. V. Gorev, S. V. Melnikova, S. V. Misjul, and V. N. Voronov, Ferroelectr. Lett. **1**, 35 (1983).
19. I. N. Flerov, M. V. Gorev, V. N. Voronov, A. Tressaud, J. Grannec, and H. Guengard, Ferroelectrics **168**, 55 (1995).
20. D. A. Erofeev, E. P. Chukalina, M. N. Popova, L. N. Bezmaternykh, and I. A. Gudim, Opt. Spectrosc. **120**, 558 (2016).
21. N. A. Teplyakova, N. V. Sidorov, S. V. Titov, I. A. Verbenko, and L. A. Reznichenko, Opt. Spectrosc. **119**, 460 (2015).
22. A. S. Krylov, E. M. Kolesnikova, L. I. Isaenko, S. N. Krylova, and A. N. Vtyurin, Cryst. Growth Des. **14**, 923 (2014).
23. I. N. Flerov, M. V. Gorev, S. V. Mel'nikova, S. V. Misyul', V. N. Voronov, K. S. Aleksandrov, A. Tresso, Zh. Grannek, Zh.-P. Shaminad, L. Rabardel', and X. Gengar, Sov. Phys. Solid State **34**, 1870 (1992).
24. V. I. Zinenko and N. G. Zamkova, Crystallogr. Rep. **49**, 29 (2004).
25. A. S. Krylov, A. N. Vtyurin, A. S. Oreshonkov, V. N. Voronov, and S. N. Krylova, J. Raman Spectrosc. **44**, 763 (2013).
26. K. S. Aleksandrov, S. V. Misyul, M. S. Molokeev, and V. N. Voronov, Phys. Solid State **51**, 2505 (2009).
27. I. N. Safonov, S. V. Misyul', M. S. Molokeev, et al., Phys. Solid State **57**, 491 (2015).

Translated by V. Rogovoi